



Normal and Superconducting Properties of $\text{Bi}_{1.7}\text{Pb}_{0.30}\text{Sr}_2\text{Ca}_{1-x}\text{La}_x\text{Cu}_2\text{O}_y$ Superconductor with $0.00 \leq x \leq 0.30$

A. Sedky¹ · Amna Salah¹ · Aly Abou-Aly²

Received: 13 April 2020 / Accepted: 25 June 2020 / Published online: 29 July 2020
© Springer Science+Business Media, LLC, part of Springer Nature 2020

Abstract

We report here normal and superconducting properties of $\text{Bi}_{1.7}\text{Pb}_{0.30}\text{Sr}_2\text{Ca}_{1-x}\text{La}_x\text{Cu}_2\text{O}_y$ superconductor with various x values ($0.00 \leq x \leq 0.30$). It is found that the replacement of Ca^{2+} by La^{3+} does not influence the phase purity of the samples, while the orthorhombic distortion, excess oxygen, effective Cu valance, and hole carriers/Cu ions are affected. Further, the doping distance and crystal geometry factor are decreased by La, but the distance between neighboring Cu atoms and the density of excess doping are increased. Furthermore, the DTA graphs show strong endothermic peaks at a temperature of 844.1, 848.03, 850.10, and 857.41 °C for pure and La-doped samples, respectively. The thermogravimetric analysis diagrams displayed a sharp mass loss started at about 800 °C and extended up to 1000 °C for all samples. Although the critical temperature T_c of the samples is decreased by La from 94 K to 83, 63, and 51 K, the critical concentration for quenching superconductivity can be extended above 0.30. Moreover, an inverse linear relation between T_m and T_c , given by T_c (K) = $-2.544 T_m$ (°C) + 2272.1, is also estimated. On the other hand, the Vickers hardness H_v is increased by La up to 0.30 ($H_v \propto T_m$, $H_v \propto (1/T_c)$), but it is decreased by the applied load F . The H_v - F characters are divided according to the applied load into two parts: the first at lower loads (0.00–1.962 N) and the second at higher loads (2.942–4.904 N). It is noted that the surface energy, elastic indentation, and resistance pressure are increased by La, but their values at higher loads are generally more than that of lower loads. Our results are discussed in terms of the balance between the hole carriers lost by La^{3+} with that introduced by excess oxygen in the Cu- O_2 planes, which alters the quenching of superconductivity by La^{3+} and highlights the present work.

Keywords 2212 phase · Resistivity · Hardness · DTA and surface energy

PACS 74.25.Bt · 74.62.Dh · 74.62.En · 74.72.gh

1 Introduction

The orthorhombic unit cell of Bi:2212 with $a \sim b = 0.544$ nm and $c = 3.090$ nm consists of two units of $(\text{Bi,Pb})_2\text{Sr}_2\text{CaCu}_2\text{O}_8$ and 15 layers. The chemical formula of 8-oxygen atoms (8O^{2-}) needs 16 electrons at least provided by $2\text{Bi}^{3+} + 2\text{Sr}^{2+} + 1\text{Ca}^{2+} + 2\text{Cu}^{2+}$ ions. To be superconductor, Bi (Pb):2212 compound should be over doped with an excess oxygen atom

δ in the range of (0.10–0.23) [1]. The extra atom requires two more electrons through transforming 2Cu^{2+} ions into 2Cu^{3+} ions, and therefore, the electronic arrangement in the unit cell becomes $2\text{Bi}^{3+} + 2\text{Sr}^{2+} + 1\text{Ca}^{2+} + 2\text{Cu}^{3+} + 9\text{O}^{2-}$.

The Bi (Pb):2212 superconducting systems with critical temperature T_c of 87 K have been early used in the fabrication of wires and tapes due to their high critical magnetic fields and critical currents [2, 3]. Bi (Pb):2212 phase is thermodynamically stable against cooling over a wide range of temperature up to 300 K [3, 4]. The partial replacement of Bi by Pb in BSCCO system has been used to stabilize the purity and formation of original 2212 phase and also to improve its superconducting critical parameters. However, the highest values of critical temperature T_c , critical field, and critical current have been obtained at $\text{Pb} = (0.20\text{--}0.30)$ [1–3]. Usually, Bi:2201 phase tends to co-exist with Bi:2212 phase during synthesis, but the calcination process helps for

✉ A. Sedky
sedky196000@hotmail.com; sedky1960@yahoo.com

¹ Physics Department, Faculty of Science, Assiut University, Assiut, Egypt

² Physics Department, Faculty of Science, Alexandria University, Alexandria, Egypt

increasing the amount of the Bi:2212 as a majority phase and depresses the amount of Bi:2201 as a minority phase [5].

The melt process is considered as the highly essential method for the behavior of thermal optimization of superconductors through solid-liquid phase diagram. Furthermore, the transition points such as melting, sublimation, and solidification can be obtained. Differential thermal analysis (DTA) and thermogravimetric analysis (TGA) are considered the best methods for identifying the above points [6]. TGA is a powerful technique to explore the thermal stability of matter through accurately monitoring the weight of the sample against heating at constant rate. The change in the sample weight during thermal treatments is attributed to the material response as a result of thermal stress. This process can be considered as the perfect way for exploring, in detail, decomposition temperatures and ensuring a material performs adequately in a given temperature range. DTA is used for measuring the temperature difference between the sample and the standard reference for obtaining solid-liquid phase diagram. However, DTA up to 1000 °C with 10 °C min⁻¹ heating rate has been used early to investigate the amount of Bi (Pb):2212 phase relative to the amounts of the other phases such as Bi (Pb):2212 phase. The DTA shows that the structure of Bi (Pb):2212 phase is more stable and can be easily prepared as stable pure phase as well as Bi (Pb):2201 phase [7].

The superconductivity of Bi (Pb):2212 system may be directly influenced by the substitution in the CuO₂ planes itself or indirectly in place of Ca²⁺ sites through affecting the charge transfer to or from that planes. However, numerous reports have been carried out on the effect of RE³⁺ substitutions in place of Ca²⁺ in Bi (Pb):2212 system (RE³⁺ rare earth element in lanthanide series) [8–15]. They approved that the replacement of Ca²⁺ by RE³⁺ in that systems decreased the hole carrier concentration, and consequently, their normal and superconducting properties are affected. It is also concluded that even though RE³⁺ improves the structural stability of the system, the superconducting critical parameters show a degrading tendency as the substitution content increases up to critical concentration x_c required for quenching superconductivity [16–18]. It is also found that x_c is decreases as the ionic size of RE³⁺ increases towards La ion in lanthanum series, while few of the reports show an improvement for these critical parameters by partial substitution of Y into Ca, Ba, and Bi sites, respectively [19–21]. Unfortunately, most of these reports have been focused on the RE³⁺ elements which already show superconductivity in the RE: 123 systems such as Y, Gd, Sm, and Nd elements, and few of them are based on La element due to poor superconductivity of La: 123. Furthermore, the superconductivity is completely quenched at $x_c = 0.25$ for substitution of La in place of Ca in (Bi,Pb):2212 systems, but it is increased above 0.25 for the other RE elements such as Y, Gd, and Nd [22–27]. Although the substitution of La³⁺ at Ca²⁺ sites in Bi (Pb):2212 shows a

depression for superconducting parameters up to 0.25, a question mark should be taken on the T_c variations by the amount of such substitution. Anyhow, the answer is still unclear and needs to pay more attention, especially with systematic La content up to 0.30.

The evaluation of mechanical properties, such as the hardness, elastic modulus, yield strength, fracture toughness, brittleness index, and ductility, is required for superconducting industrial applications such as quasi-permanent magnets and current loads. According to the geometry of indenter and size of applied load, Vickers microhardness has been used to investigate the mechanical properties of solids in the form of bulk samples. Generally, indentation size effect (ISE) occurs when the microhardness decreases as the applied load increases [28, 29], while the reverse indentation size effect occurs when the microhardness increases with the applied load [30–32]. Generally, the high T_c superconductors have relatively poor mechanical properties, which limit as possible their practical applications. One of the important strategies to improve these properties is the substitution process. For example, it is found that RE³⁺ substitution in place of Ca²⁺ improves the connection between superconducting grains, and consequently, the mechanical resistance has increased [33–35].

As a continuation of the above work, and to understand more about the influence of La³⁺ substitution at Ca²⁺ site in Bi_{1.7}Pb_{0.30}Sr₂Ca_{1-x}La_xCu₂O_y samples, a systematic study on the structural, DTA, TGA, mechanical, and superconducting analyses with various x values ($0.00 \leq x \leq 0.30$) is reported. On the light of the present work, it is approved that although the superconducting critical temperatures are decreased by La, the x_c for quenching superconductivity can be extended above 0.30. Furthermore, the decomposition temperature, hole carries/Cu ions, and Vickers hardness are increased by La up to 0.30. However, these findings are discussed in terms of the correlation between the hole carriers lost by La with that introduced due to excess oxygen resulting for increasing the x_c and solubility of La³⁺, which highlights the present work.

2 Experimental Details

The Bi₂O₃, PbO, SrO, La₂O₃, CaCO₃, and CuO oxides and carbonates of 4N purity (Bi,Pb)₂Sr₂Ca_{1-x}La_xCu₂O_y) are thoroughly mixed in required proportions and calcined at 825 °C in air for 24 h. This exercise is repeated three times with intermediate grinding at each stage. The resulting powder was reground, mixed, and pressed into pellets at a force up to 10 tons and sintered in air at 840 °C for 36 h and left in the furnace for slow cooling to room temperature by a rate of 5°/min. For more and more optimization of excess oxygen in the samples, the pellets are annealed in air at 850 °C for 20 h and left in the furnace for slow cooling to room temperature. The

phase purity of the samples in powder form is examined by using X-ray diffraction (XRD). DTA and TGA of the samples in powder form are performed in the temperature range (30–1000 °C) with heating rate of 10 °C/min. The melting behaviors of the samples are analyzed by Shimadzu differential thermal analysis-50 (DTA). The electrical resistivity of the samples is obtained using the standard four-probe technique in closed cycle cryogenic refrigerator within the range of 18–300 K (Displex) employing helium gas. A 1.0-mA dc current, I , is supplied by a digital Keithley 6221 constant current source, and the dc voltage drop, V , is measured by using dc Keithley 181 digital nanovoltmeter in the normal and reverse directions across the samples. A calibrated chromel versus gold with 0.07 at % iron (Kp-Au 0.07 at % Fe) thermocouple is used for recording the temperature of the sample. The electrical resistivity of the samples is obtained using the relation, $\rho = \frac{Vwt}{IL}$, where w , L , and t are the samples width, length, and thickness, respectively. Finally, the Vickers microhardness of the samples at room temperature is determined using manual microhardness tester model IN-412A with an applied loads of (0.49–10 N) for 10 s.

3 Results and Discussion

3.1 Structural Analysis

The calculated and measured values of density ρ_{th} and ρ_{exp} for the samples are listed in Table 1. It is clear that ρ_{th} and ρ_{exp} are gradually increased by La, but the values of ρ_{exp} are higher than that of ρ_{th} . The increase of ρ by La may be related to the amount of excess oxygen produced during sample synthesis. The porosity of the samples is calculated using the following relation: $PS = [1 - (\rho_{exp}/\rho_{th})]$ and is listed also in Table 1 [6, 36]. The values of PS are gradually decreased by La, which is probably related to decreasing the number of pores due the effective hole carriers as a result for La substitution. It is evident from XRD pattern shown in Fig. 1 that all samples are

single phase and free from any impurity phases. The obtained peaks are identified by 2212 (hkl)_H and 2201 (hkl)_L as majority and minority superconducting phases, respectively [37, 38]. The hkl peaks of high intensities indicated by H belong to the studied Bi (Pb):2212 high phase ($T_c = 87$ K), while the hkl peaks of lower intensities indicated by L belong to Bi (Pb):2201 low phase ($T_c = 23$ K). However, the composition of low 2201 superconducting phase is (Bi,Pb)₂Sr₂CuO₆, and it is normally formed as minority phase and cannot be consider as impurity phase as well as the minority 2212 phase formed in 2223 phase. However, there are only four peaks formed and related to 2201 such as (113), (115), (019), and (033).

The volume fraction of the Bi (Pb):2212 superconducting phase (V_{2212}) of the samples is determined by using the following relation [39, 40]:

$$V_{2212} = \frac{\Sigma I_{2212}(\text{peaks})}{\Sigma I_{2212}(\text{peaks}) + \Sigma I_{2201}(\text{peaks}) + \Sigma I_{\text{other}}(\text{peaks})} \tag{1}$$

where I_{2212} , I_{2201} , and I_{other} are the intensities of peaks for 2212, 2201, and impurity phases, respectively. As listed in Table 1, a little bit decrease of the V_{2212} by La up to 0.15 followed by an increase with further more increase of La up to 0.30 is obtained. The $V_{2212}\%$ of the samples is 92.8%, 92.3%, 92.3%, and 96%, respectively.

The average crystallite diameter D_{hkl} is evaluated by the following Scherer equation [41–43]:

$$D_{hkl} = \frac{k\lambda}{\Delta\theta\cos\theta} \tag{2}$$

where λ is the X-ray wavelength ($\lambda = 1.5418 \text{ \AA}$), $\Delta\theta$ is the half maximum line width, θ is the Bragg angle, and k is constant ($k = 0.93$ for most of ceramic materials). By using the Lorentz

Table 1 Lattice parameters, c/a , OD, D , β , $V_{2212}\%$, ρ , and PS for pure and La samples

La cont.	a (Å)	b (Å)	c (Å)	c/a	OD	$V_{2212}\%$
0.00	5.383	5.412	30.764	5.716	0.0054	92.8%
0.05	5.393	5.404	30.784	5.709	0.0021	92.3%
0.15	5.397	5.406	30.782	5.704	0.0018	92.3%
0.30	5.386	5.415	30.776	5.714	0.0054	96.0%
La cont.	D (nm)	β (nm) ⁻²	ρ_{exp} (g/cm ³)	ρ_{th} (g/cm ³)	PS	
0.00	18.67	0.0029	5.11	5.42	0.057	
0.05	19.03	0.0028	5.19	5.40	0.039	
0.15	22.87	0.0019	5.26	5.43	0.031	
0.30	25.81	0.0015	5.35	5.51	0.029	

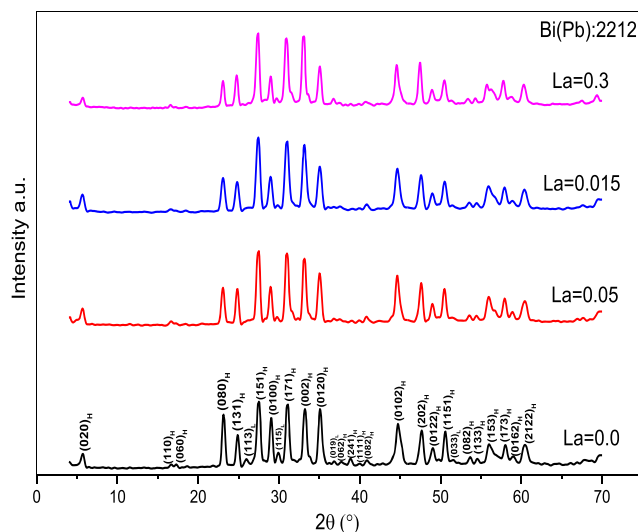


Fig. 1 XRD patterns for pure and La the samples (H and L indicate to Bi (Pb)2212 and Bi (Pb) 2201 phases)

Table 2 y , Cu^{eff} , d , Z , and CGF for the samples

La cont.	y	Cu^{eff}	$\Sigma^{1/2}$	Σ^{-1}	d (Å)	Z (Å)	CGF
0.00	8.096	2.246	9.183	0.012	49.434	12.036	51.2E-70
0.05	8.168	2.293	6.973	0.021	37.604	12.059	26.8E-70
0.15	8.473	2.548	4.232	0.056	22.842	12.068	7.30E-70
0.30	8.575	2.575	3.862	0.067	20.799	12.043	4.87E-70

square method, values of D_{hkl} listed in Table 1 are 18.76, 22.87, 19.03, and 25.93 nm for pure and La samples, respectively. The dislocation density (β) calculated by, $\beta = 1/D^2$, and listed in Table 1 is between 0.0029 and 0.0015 for all samples, which indicates that the samples have very few lattice defects and good crystalline quality as obtained by XRD [44].

The variations of lattice parameters a , b , and c listed in Table 1 indicated that b and c/a are slightly decreased by La up to 0.15 followed by an increase at 0.30, while a little bit simultaneous expansion along the c -axis is obtained followed by a decrease at 0.30. The behavior of orthorhombic distortion $\text{OD} = (b - a)/a$ listed in Table 1 is similar to b and c/a variations. This is due to the difference between the ionic radii between La^{3+} ions (1.18 Å) and Ca^{2+} (1.12 Å) at the same 8-fold coordination. However, the unusual behavior for the above parameters against La content is often related to the excess of oxygen inserted into BiO layers and also the Cu-O bonding in the Cu-O planes as reported elsewhere [20, 22, 45]. The ratio (c/a) is generally used to characterize the Jahn-Teller distortion of the oxygen octahedron around Cu^{2+} , and therefore, a systematic change of c/a by La content indicates that La release the Jahn-Teller distortion of the CuO_6 octahedron markedly [46, 47].

The oxygen content y of superconducting systems can be obtained by titration in terms of a parameter H using the following formula [48]:

$$H = \left[\left(\frac{V_1 m_2}{V_2 m_1} \right) - 1 \right]; y = 8 + 1.5H \quad (3)$$

where V_1 , V_2 , m_1 , and m_2 are the volumes of $\text{Na}_2\text{S}_2\text{O}_3$ solutions and masses of the sample during the first and second titration, respectively. The values of y listed in Table 2 for

the samples are increased from 8.096 for pure sample to 8.168, 8.473, and 8.575 for La samples, respectively. This behavior indicated that La helps for more excess of oxygen to the La free system. On the other hand, the effective Cu^{eff} valance can be also obtained with the help of the valence state of the composition elements (Bi^{+3} , Pb^{+2} , Sr^{+2} , Ca^{+2} , La^{+3} , and O^{-2}) as $3 \times 1.7 + 2 \times 0.3 + 2 \times 2 + 2(1-x) + 3x + 2\text{Cu}^{\text{eff}} = 2y$, using the following relation:

$$\text{Cu}^{\text{eff}} = \frac{2y - [9.7 + 2(1-x) + 3x]}{2} \quad (4)$$

where x is the La content. The values of Cu^{eff} listed in Table 2 are also increased by La as well as y . It is increased from 2.246 for pure sample to 2.293, 2.548, and 2.575 for La samples, respectively.

However, the formation of 2212 high T_c requires the existence of Cu^{3+} ions in the form of excess oxygen in/or near to the CuO_2 planes [26, 49, 50]. It is believed that the Coulomb potential caused by the excess oxygen atoms pins the doped holes in the CuO_2 planes so as to minimize their total energy [51]. It is found that the excess oxygen atoms introduced in the system have been transformed into a distance assuming a uniform density of excess oxygen positions in the CuO_2 planes. This has been done by representing a unit area for one doping element as a square planar configuration. The considered unit area is formed by four doping elements at each corner and having Σ elements. The density of excess doping Σ^{-1} in Bi:2212 system is given by $\Sigma^{-1} = (1 - 8y^{-1})$ relation, where Σ is the doping density [52, 53]. The excess oxygen can be also converted into a doping distance d given by $d = a\sqrt{\Sigma}$. Furthermore, the distance z between any two neighboring Cu atoms in the designated direction can be calculated in terms of a parameter by $z = \sqrt{[(2a)^2 + a^2]} = a\sqrt{5}$. Moreover, the crystal geometry factor (CGF) of the superconducting planes area can be obtained by the following [51–53]:

$$\text{CGF (Jm}^2 \text{ kg)} = [(2d)^2 n^{\frac{3}{2}} 2\pi K_B T_c m_{\text{eff}}] = 6.31 \times 10^{-54} d^2 T_c n^{\frac{3}{2}} \quad (5)$$

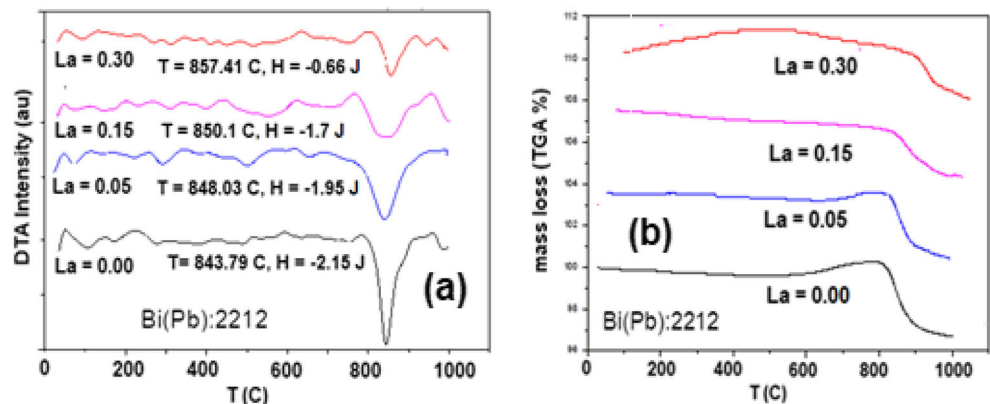
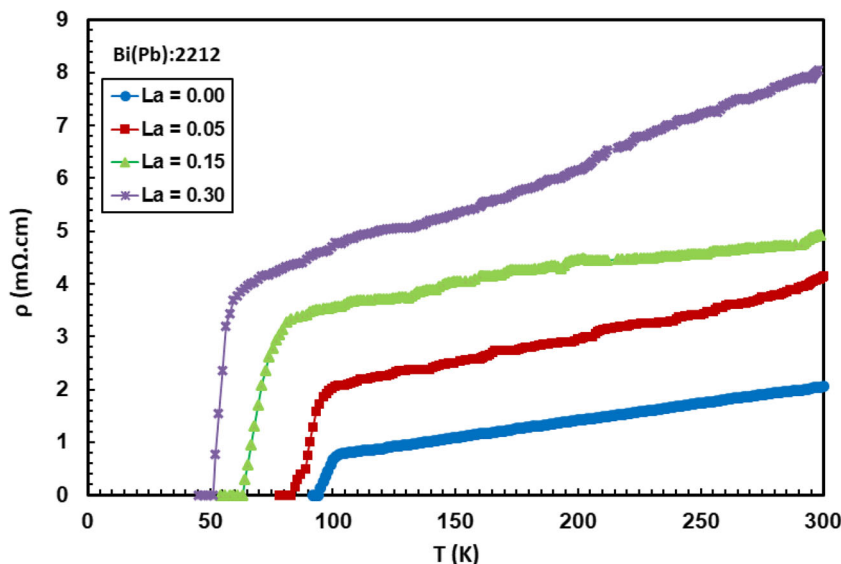
Fig. 2 a, b DTA and TGA curves for pure and La the samples

Fig. 3 Resistivity versus temperature curves for pure and La the samples



where n is the number of CuO_2 planes ($n = 2$ for 2212) and m_{eff} is the effective mass of the hole-doped cuprates ($m_{\text{eff}} = 2m_e = 18.2 \times 10^{-31}$ kg). We therefore simply apply the above relations for the samples to check the response of La to the pure system. The values of d , Σ^{-1} , z , and CGF listed in Table 2 indicated that d and CGF are decreased by La, while z and Σ^{-1} are slightly increased. Decreasing the doping distance d along with increasing the density of excess doping z by La is considered the good evidence for increasing the hole carrier concentration of the system.

3.2 DTA and TGA

Figure 2a shows the DTA patterns of the pure and La samples. It is evident from the figure that with increasing temperature above RT, there are some exothermic and endothermic peaks observed and gradually shifted to higher temperature as La increases. They occurred at temperature ranges of 30–200 °C, 200–450 °C, 450–700 °C, and 650–800 °C for the samples, respectively. This is corresponding to crystallizations of 2201, 2212, and $(\text{Sr,Ca})_2\text{CuO}_3$ phases, and also due to transformation of 2201 phase to 2212 phase. With increasing temperature at about 800 °C, the tendencies of 2201 crystallization phase decrease and completely disappear. Interestingly, the strong endothermic peaks occurred only at a temperature of 844.1,

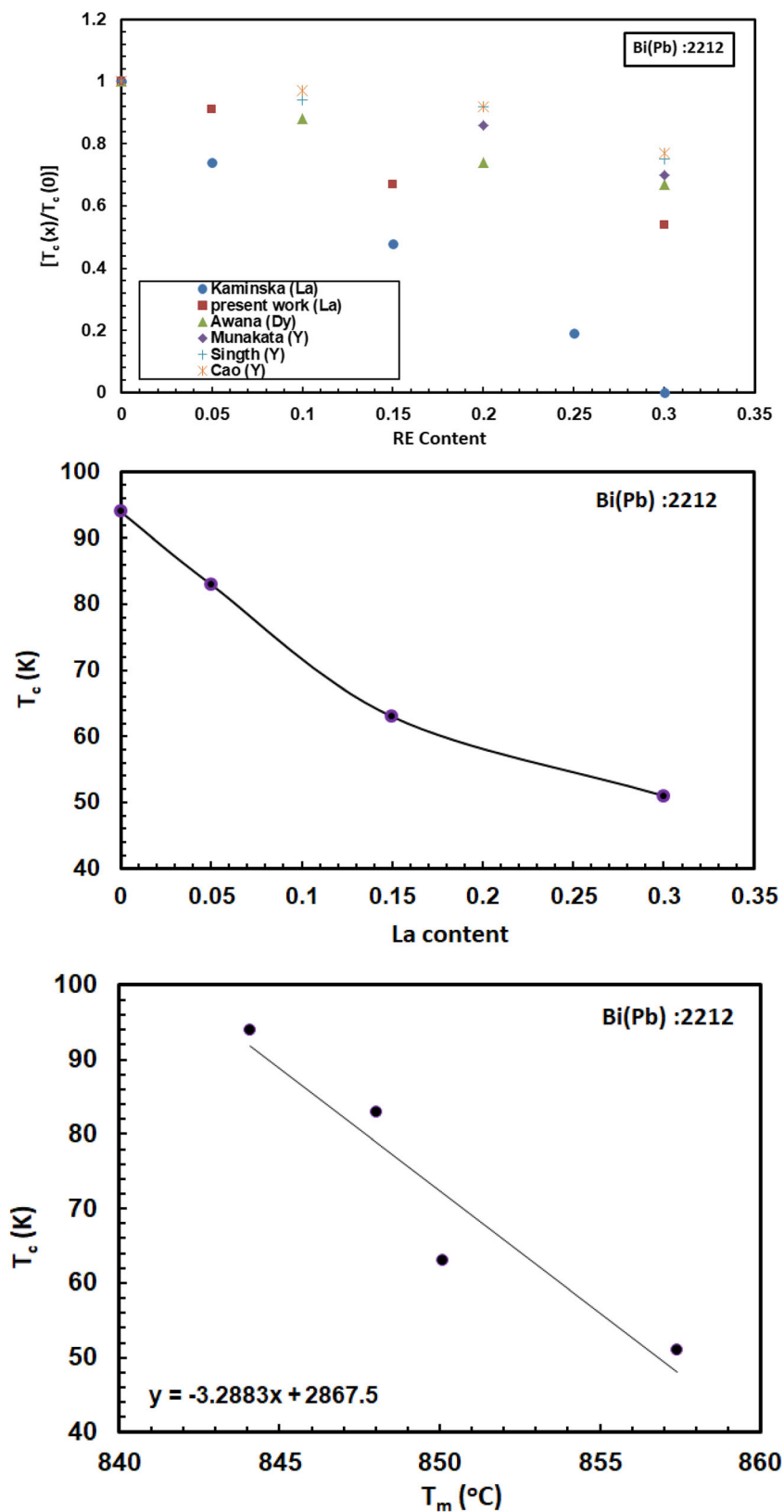
848.03, 850.10, and 857.41 °C, and no any other strong peaks could be observed which reinforce the purity of the samples as indicated by XRD. This is due to decomposition reaction of 2212 superconducting phase, and it is usually attributed to the increase of optimum temperature of the mixture due to La, which facilitates the growth of 2212 phase. Such observed increase in T_m emphasizes the role of La addition on the internal structure of the examined samples. Furthermore, the endothermic heats recorded at the endothermic peaks listed in Table 2 are decreased from 2.15 J for pure sample to 1.95, 1.7, and 0.66 J for La samples, respectively. This obtained result claimed that the 2201 phase melts above 800 °C, and after that, it decomposes into 2212 phase, as reported elsewhere [54, 55]. These results indicated that La improves the melting point of 2212 without producing any other additional compound.

The mass loss was determined by TGA shown in Fig. 2b indicating that the samples ($x = 0.00, 0.05, \text{ and } 0.15$) displayed a gradual quite of mass loss starting above a temperature of 30 °C to about 450, 600, and 800 °C, followed by a mass gain and then followed by a sharp mass loss at about 800 °C. However, the period of mass gain completely disappears for La = 0.15 sample. But with increasing La up to 0.30, a gradual mass gain occurs with increasing temperature form 35 °C up to 500 °C, followed by a sharp mass loss up to 1000 °C. It is obvious that gradual mass loss is due to de-oxidization, while

Table 3 T_m , heat at the peak, ΔT (°C), and mass loss (%) for the samples

La cont.	T_m (°C) (DTA)	DTA heat at peak (J)	ΔT (°C) TGA	TGA mass loss (%)	ΔT (°C) TGA	TGA mass loss (%)
0.00	844.51	−2.15	(44–624)	−0.207	(627–991)	−3.046
0.05	848.03	−1.95	(32–613)	−0.408	(617–993)	−3.114
0.15	850.10	−1.70	(33–686)	−0.735	(691–991)	−2.538
0.30	857.41	−0.66	(35–700)	+0.371	(706–995)	−2.759

Fig. 4 **a** $[T_c(x)/T_c(0)]$ versus RE content for the present and reported data. **b** T_c versus La content for pure and La the samples. **c** T_c versus T_m for pure and La the samples



the mass gain is due oxidation. It is clear that La has an effect on the starting temperature of mass loss and also mass gain. The temperature at which the mass gain begins is shifted to

higher values as La increases up to 0.15. Anyhow, a sharp mass gain close to 800 $^{\circ}$ C may be due to the decomposition temperature as indicated by DTA analysis. Increasing the

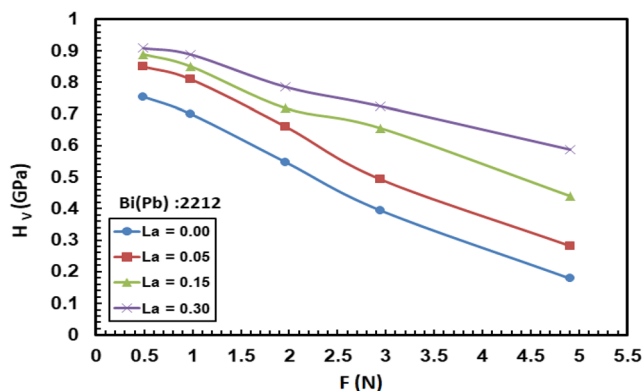


Fig. 5 Measured hardness against applied load for pure and La samples

mass loss/mass gain by La is related to the excess of oxygen as discussed above. Consequently, the sample takes more oxygen atoms to fill these oxygen deficiencies [6, 7, 56]. Interestingly, the oxygen content y of the samples is calculated for Y:123 with the help of TGA analysis using the following empirical relation [57];

$$y = \left(\alpha + \frac{x}{2}\right) + \frac{\ell}{m-\ell} \left(\frac{M}{16}\right) \tag{6}$$

where α is a parameter ($\alpha = 3.5$) for Y:123 systems, x is the doping content, m is the mass of the sample, ℓ is the average mass loss, and M is the atomic weight. Substituting by the values of ℓ , M , and m deduced from TGA, and y from titration method, we found that $\alpha = 6.5$ for 2212 system.

3.3 Resistivity Measurements

Figure 3 depicts the resistivity versus temperature for pure and La samples. From this figure, it can be observed that the resistivity decreases almost linearly from room temperature and beyond which it turns to zero at a critical temperature T_c . It is also noted that all samples exhibit a clear metallicity and the linear part of curves from RT down to onset temperature has a positive slope $d\rho/dT$ and its extrapolation to $T = 0$ K provides the residual resistivity ρ_0 . Usually, ρ_0 is related with impurity scattering, while $d\rho/dT$ is related with carrier-carrier scattering

[58]. However, the resistivity drop occurred in a single step for pure sample as indicated in the figure implying a single phase, while La samples have broadened the width of transition temperature, ΔT_c [59]. However, the values of ρ_{300} , ρ_0 , and ΔT_c presented in Table 3 are increased by La, but $d\rho/dT$ is decreased. Furthermore, the T_c is observed at 94 K for pure sample, but it is decreased to 85, 63, and 51 K for La samples.

We would like to mention here about the substitution of RE^{3+} in place of Ca^{2+} in Bi (Pb):2212 system [8–21]. The reported data of the reduced critical temperature [$T_c(x)/T_c(0)$] against rare earth elements are drawn and shown in Fig. 4a, and the present data are enclosed for comparison. This behavior indicated that La^{3+} , compared with the other rare earth elements of lower ionic size such as Y and Dy, has nearly a similar behavior. But the present work is less detrimental to the superconductivity as compared to the reported for La as indicated in the figure. On the other hand, it is evident from the Fig. 4a that the critical concentration x_c of La required for quenching superconductivity can be extended above 0.30 rather than the reported (0.25). However, different solubilities of rare-earth element R^{3+} in Bi (Pb):2212 system can be understood by a comparison of their ionic radii of 1.02, 1.03, and 1.18 Å at 8-fold coordination for Y, Dy, and La with respect to 1.12 Å of Ca^{2+} [60]. It is approved that the solubility has decreased as one move towards the right in lanthanide series such as La, which is not obtained in the present work. An inverse linear relation between T_m and T_c is obtained in Fig. 4c and given by T_c (K) = $-3.29 T_m + 2867.5$. This is completely consistent with the reported data for the inverse linear relation between T_c and T_m for Y:123, Bi:2223, and Ti:2223 superconducting systems [61]. Although the T_c values are respectively 92, 110, and 125 K for these systems, the values of T_m are 1010, 867, and 807 °C, respectively. This finding suggests that in order to get higher T_c , a eutectic compound of lower melting point should be looked forward.

The phase diagram of high T_c systems is well described by the parabolic relation [62]:

$$\frac{T_c^m}{T_c^x} = 1 - 82.6(p - 0.16)^2 \tag{7}$$

Fig. 6 a, b Young’s modulus and Yield strength against applied load for pure and La samples

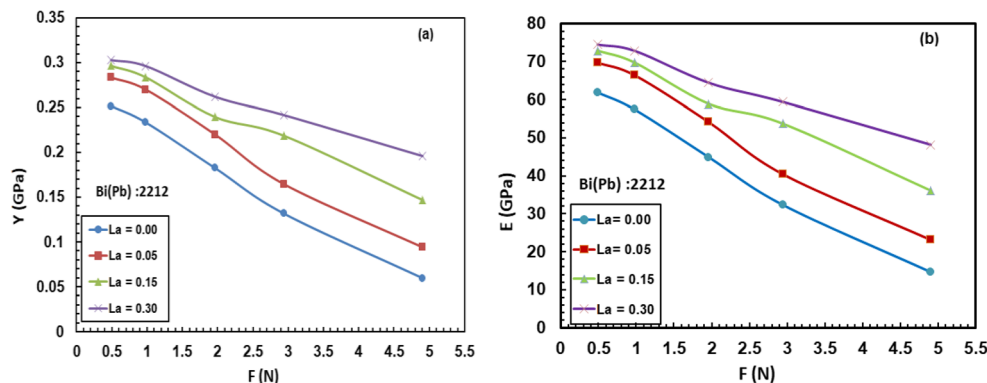
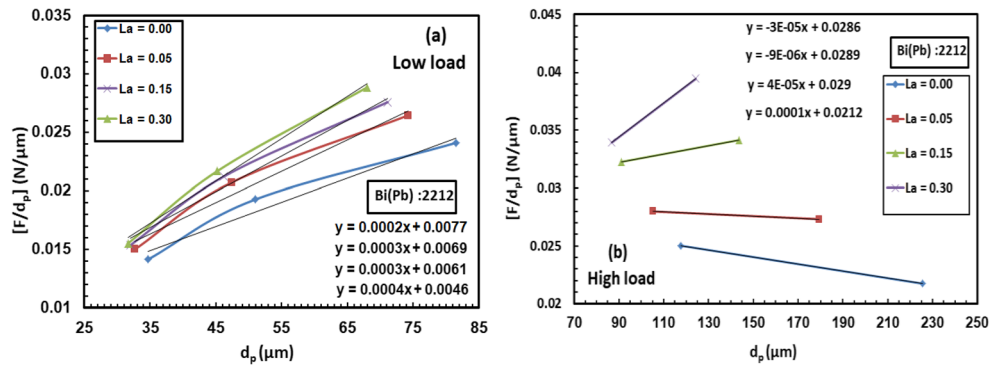


Fig. 7 a, b The plot of F/d_p against d_p at lower load for pure and La samples



where T_c^{im} is the maximum critical temperature of the pure sample (94 K) and T_c^x is the critical temperature of the La samples. p is the hole-carrier concentration per Cu ion. It is clear from Table 2 that p is increased from 0.16 for pure sample to 0.19, 0.22, and 0.23 for La samples, respectively. This behavior occurs as a result of more positive charges transferred by La to the CuO_2 planes. But this disagree with the general role of substitution as a result of replacing Ca^{2+} by La^{+3} , and therefore, p , should be to decreased. According to the mechanism of the excess of oxygen in BSCCO system, the electrons are transferred from Cu sites to BiO layer leading to the formation of holes on the Cu and electrons on the Bi as follows: $Bi^{3+} + Cu^{2+} \rightarrow Bi^{3-x} + Cu^{2+x}$ [63]. These aforesaid changes in the valence state of Bi are reflected due to the change of hole carriers owing to the excess of oxygen. To clarify this point according the role of substitution, we supposed that La^{3+} decreased the density of hole carriers, and at the same time, the excess of oxygen introduced some excess of holes in the Cu- O_2 planes, and consequently, the effective (net) number of holes will be increased. This can be also supported by decreasing the doping distance and increasing the excess oxygen as discussed in the above paragraph.

3.4 Microhardness Measurements

The Vickers microhardness H_v at different loads for the samples is calculated by the following relation [64]:

$$H_v = 1854.4 \left(\frac{F}{d_p^2} \right) \tag{8}$$

where H_v is given by GPa, d_p is the diagonal length of the indentation by micrometers, and F is the applied load by N

($F = 0.49, 0.981, 1.962, 2.942,$ and 4.904 N). It is obvious from the curves of H_v versus F shown in Fig. 5 that H_v values are decreased by increasing F up to 4.904 N. This behavior is usually due to increasing the penetration depth where the inner layer effect becomes more prominent as discussed above (the well-known indentation size effect). Interestingly, at constant F , the values of H_v are increased by La, which can be attributed to decreasing the impurities and also increasing the density of the samples as listed in Table 1. This helps for improving the connectivity between the superconducting grains, and consequently, H_v has improved. The elastic Young’s modulus E and yield strength Y are related to the H_v as follows [65, 66]:

$$E = 81.9653H_v; Y = \left(\frac{H_v}{3} \right) \tag{9}$$

However, a similar behavior of both E and Y against F could be obtained and shown in Fig. 6a, b. This is probably due improving the roughness and interlayer bonding of superconducting grains when Ca is replaced by La.

The diagonal length d_p is strongly dependent on the applied load F according to the following relation [22, 67–69]:

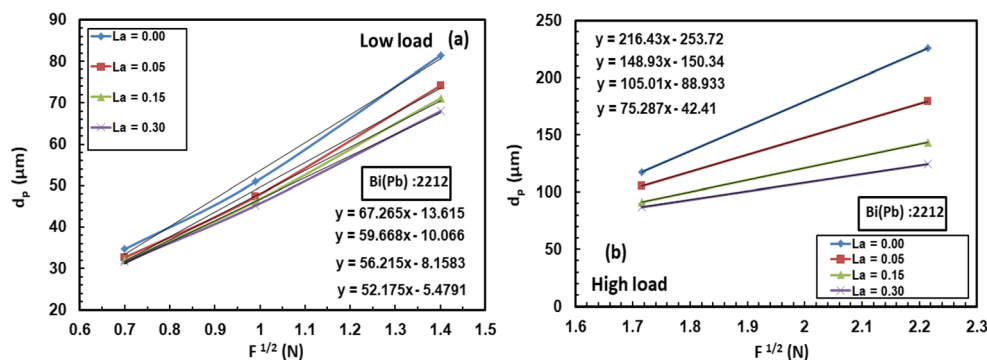
$$\frac{F}{d_p} = H_t d_p + \gamma \tag{10}$$

where H_t is the true hardness and γ is the surface energy. As a result of unsystematic linear behavior for the lines, the character is divided into lower and higher loads for simplicity. The plots of (F/d_p) against d_p for the lower and higher loads are shown in Fig. 7a, b where the slope represents H_t and the intercept represents γ . Interestingly, the slope of the linear plot is positive for all samples at lower loads (0.00–1.962 N). While at higher loads, the slope is

Table 4 $\rho_{300}, \rho_o, dp/dT, T_c, T_{on}, T_c(x)/T_c(0), \Delta T_c,$ and p for samples

La content	ρ_{300} (mΩ cm)	ρ_o (mΩ cm)	dp/dT (mΩ cm/K)	T_c (K)	T_{on} (K)	ΔT_c (K)	p
0.00	2.06	0.40	0.0065	94	103	9	0.16
0.05	4.15	1.15	0.010	83	99	13	0.19
0.15	4.93	2.85	0.007	63	80	17	0.22
0.30	13.39	5	0.027	51	65	14	0.23

Fig. 8 **a, b** Measured indentation against loads for pure and La samples



negative for La = 0.00 and 0.05 samples and changed to positive for La = 0.15 and 0.30 samples. However, the different values of H_t and γ are listed in Table 4. It is clear that H_t has a similar behavior of H_v , which indicates a decrease of crack faces by La and supports the hardness improvements. But the values of γ are generally decreased from 0.029 N/ μm to 0.021 N/ μm for pure sample at higher loads, and from 0.008 to 0.005 N/ μm at lower loads. From atomistic point of view, the more compacted surface the higher hardness and thus having lower surface energy.

The indentation size effect can be explained by two different methods [70–73]. The first method assumes that the indentation contains an elastic portion of the deformation which is supposed to relax upon the load beside plastic deformation. This can be accounted by adding an elastic component d_e to the measured elastic component d_p , supposing that they are in the same direction, as follows [28, 74]:

$$H_t = 1854.4 \left[\frac{F}{(d_p + d_e)^2} \right] \tag{11}$$

$$d_p = \left[\left(\frac{1854.4}{H_t} \right)^{\frac{1}{2}} F^{\frac{1}{2}} - d_e \right]^2$$

The plot of d_p versus $F^{1/2}$ at lower and higher loads is shown in Fig. 8a, b, in which the slope represents

$[(1854.4)^{1/2}(H_t)^{-1/2}]$, and the vertical intercept represents the d_e . The values d_e listed in Table 5 are generally decreased by La which emphasizes the hardness suppression as discussed above. Furthermore, the values of d_e at higher loads are higher than that of lower loads. At lower loads, d_e is decreased from 13.62 μm for pure sample to 10.07, 8.16, and 5.48 μm for La samples and from 253.72 to 150.34, 88.93, and 42.41 μm at higher loads.

The second method considers the effect of energy dissipative processes, and therefore, the H_t can be defined by subtracting the dissipative part F_o from the applied load F as follows [75]:

$$H_t = 1854.4 \left(\frac{F - F_o}{d_p^2} \right) \tag{12}$$

$$F = \left(\frac{H_t}{1854.4} \right) d_p^2 + F_o$$

The slope of linear plot of F against d_p^2 is shown in Fig. 9a, b, in which $(H_t/1854.4)$ represents the slope and the intercept represents the resistance pressure F_o . The values of F_o listed in Table 5 are decreased by La, but at higher loads, they are more than that of lower loads (F_o (HL) = 10 F_o (LL)). It is decreased at lower load from 0.22 for pure sample to 0.19, 0.16, and 0.12 N and from 2.21 to 1.92, 1.62, and 1.08 N at higher loads.

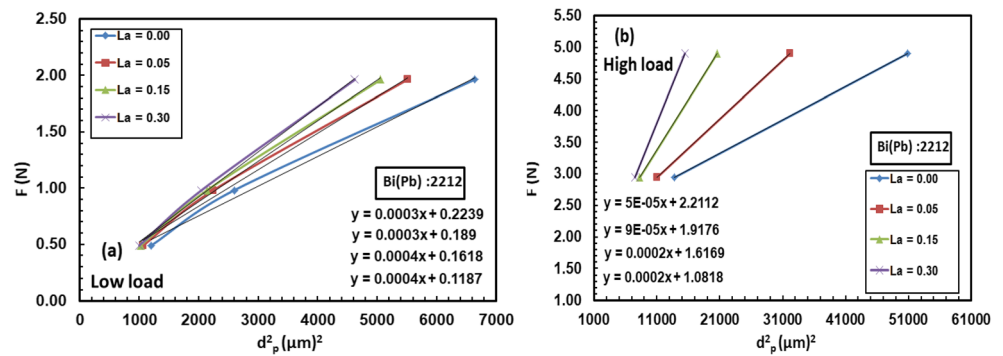
However, the following points are obtained due substitution of La in place of Ca in Bi (Pb):2212 superconducting phase: (i) A clear 2212 majority superconducting single phase; (ii) increasing the density, c-parameter, and excess of oxygen; (iii) decreasing orthorhombic distortion, doping distance, and crystal geometry factor; (iv) increasing the distance between Cu atoms, density of excess doping, hole carriers per Cu ion, effective Cu valence, critical concentration for quenching superconductivity, and hardness; (v) shifting endothermic peaks to higher temperatures; (vi) a sharp of mass loss starting at about 800 °C; (vii) decreasing the critical temperature, surface energy, resistance pressure, and elastin indentation.

In the above background, the following points are concluded. Firstly, the T_c depression is not related to the phase purity or bad microstructure in the form of secondary phases rich in

Table 5 H_t , γ , d_e , and F_o for pure and La samples

La cont.	H_t (GPa)	γ (N/m)	d_e (μm)	F_o (N)
Low loads				
0.00	0.371	0.008	13.62	0.22
0.05	0.556	0.007	10.07	0.19
0.15	0.556	0.006	8.16	0.16
0.30	0.742	0.005	5.48	0.12
High loads				
0.00	-0.056	0.029	253.72	2.21
0.05	-0.017	0.029	150.34	1.92
0.15	0.074	0.029	88.93	1.62
0.30	0.185	0.021	42.41	1.08

Fig. 9 a, b Applied load against elastic indentation for pure and La samples



Sr [76–78]. Secondly, although La decreased the hole carriers, the excess oxygen is more than enough to compensate the variation of charge in the system, and consequently, the number of holes in the CuO_2 planes increases. The balance between the hole carriers lost by La^{3+} with that introduced by the excess of oxygen results in increasing the effective (net) of hole carriers, which can be considered as the possible reason for altering the quenching of superconductivity by La^{3+} in the present work. However, the consistency of these points gave us a fair degree of certainty to the suggestion of La substitution in place of Ca in Bi (Pb):2212 system.

4 Conclusion

Structural and normal properties of $\text{Bi}_{1.7}\text{Pb}_{0.30}\text{Sr}_2\text{Ca}_{1-x}\text{La}_x\text{Cu}_2\text{O}_y$ superconductor with various x values ($0.00 \leq x \leq 0.30$) are investigated. We have shown that the replacement of Ca^{2+} by La^{3+} increased the excess of oxygen, effective Cu valance, and hole carrier per Cu ion. Further, the doping distance and crystal geometry factor are slightly decreased, while the distance between Cu atoms and the density of excess doping are increased. Furthermore, a strong shift of endothermic peaks to higher temperatures and also a sharp mass loss is obtained. Although the critical temperatures T_c are decreased by La, the critical concentration for quenching superconductivity x_c can be extended above 0.30. Moreover, an inverse linear relation between T_m and T_c given by T_c (K) = $-3.29T_m$ (°C) + 2867.50 could be obtained. On the other hand, Vickers hardness H_v is decreased by the applied loads F , but it is increased by La ($H_v \propto T_m$, $H_v \propto (1/T_c)$), and the H_v - F character could be divided into lower and higher loads. The surface energy, resistance pressure, and elastic indentation are generally decreased by La, and their values at higher loads are more than that of lower loads. The balance between the hole carriers lost by La^{3+} with that introduced by excess of oxygen resulting for increasing the effective (net) of hole carriers can be considered as the possible reason for altering the quenching of superconductivity by La^{3+} which highlights the present work.

References

- Eisaki, H., Kaneko, N., Feng, D.L., Damascelli, A., Mang, P.K., Shen, K.M., Shen, Z.X., Greven, M.: Phys. Rev. B. **69**, 064512 (2004)
- Jeremie, A., Yadri, K.A., Grivel, J.C., Fikiger, R.: Supercond. Sci. Technol. **6**, 730 (1993)
- Maeda, H., Tanaka, Y., Fukutomi, M., Asano, T.: Jpn. J. Appl. Phys. **27**(2), L209 (1988)
- Amirabadizadeh, A., Memarzadeh, S., Tajabor, N., Arabi, H.: World J. Condens. Matter Phys. **2**, 148 (2012)
- Gul, I.H., Rehman, M.A., Ali, M., Maqsood, A.: Phys. C. **432**(1–2), 71 (2005)
- Aksan, M.A., Yakinci, M.E.: J. Alloys Compd. **433**, 22 (2007)
- Hwang, C.H., Kim, G.: Supercond. Sci. Technol. **5**, 586 (1992)
- dos Santos, C.A.M., Moehlecke, S., Kopelevich, Y., Machado, A.J.S.: Physica C. **390**, 21 (2003)
- Lu, X.G., Zhao, X., Fan, X.J., Sun, X.F., Wu, W.B., Zhang, H.: Appl. Phys. Lett. **76**, 3088 (2000)
- Ilyushchkin, A.Y., Yamashita, T., Boskovic, L., Mackinnon, I.D.R.: Supercond. Sci. Technol. **17**, 1201 (2004)
- Jassim, K.A., Tariq, J., Alwan, J.: Supercond. Nov. Magn. **22**, 861 (2009)
- Singh, S.: Physica C. **294**, 249 (1998)
- Nanda Kishore, K., Satyavathi, S., Muralidhar, M., Pena, O., Hari Babu, V.: Physica C. **252**, 49 (1995)
- Sedky, A.: J. Phys. Chem. Solids. **70**, 483 (2009)
- Marconi, D., Stiufiuc, G., Pop, A.V.: J. Phys. Conf. Ser. **153**, 012022 (2009)
- Hudakova, N.: Physica C. **406**, 58 (2004)
- dos Santos, A.D.M., Pinto, G.S., Ferreira, B., Machado, A.J.S.: Physica C. **354**, 388 (2001)
- Cao, Q., Ruan, K.Q., Li, S.Y., Chen, X.H., Qian, G.G., Cao, L.Z.: Physica C. **334**, 237 (2000)
- Khalil, S.M.: J. Phys. Chem. Solids. **64**, 855 (2003)
- Sun, X., Zhao, X., Wu, W., Fan, X., Li, X.-G., Ku, H.C.: Physica C. **307**, 7 (1998)
- Awana, V.P.S., Agarwal, S.K., Ray, R., Gupta, S., Narlikar, A.V.: Physica C. **43**, 191 (1992)
- Yilmazlar, M., Cetinkara, H.A., Nursoy, M., Ozturk, O., Terzioğlu, C.: Physica C. **442**, 101 (2006)
- Sedky, A.: Physica C. **468**, 1041 (2008)
- Sale, F.R., Mahloojchi, F.: Ceram. Int. **14**, 229 (1988)
- Yanru, R., Hanpeng, L., Mingzhu, L., Qingyun, T., Lihua, S., Zhenjin, L., Xianren, M.: Physica. **156**(5), 799 (1988)
- Hwang, J., Timusk, T., Gu, G.D.: Nature. **427**, 714 (2004)
- Norman, M.: Nature. **427**, 692 (2004)
- Gong, J., Wu, J., Guan, Z.: J. Eur. Ceram. Soc. **19**(15), 2625 (1999)
- Khalil, S.M.: J. Phys. Chem. Solids. **62**(3), 457 (2001)
- Elmustafa, A.A., Stone, D.S.: J. Mech. Phys. Solid. **51**, 357 (2003)

31. Sangwal, K.: *Mater. Chem. Phys.* **63**, 145 (2000)
32. Musa Abbas, M.: *Int. J. Curr. Eng. Tech.* **5**(3), 1908 (2015)
33. Khalil, S.M.: *Smart Mater. Struct.* **14**, 804 (2005)
34. Schuller, I.K., Jorgensen, J.D.: *MRS Bull.* **14**, 27 (1989)
35. Ravinder, D., Alivelu Manga, T.: *J. Alloys Compd.* **299**, 5 (2000)
36. Khalil, S.M., Sedky, A.: *Physica B.* **357**, 299 (2005)
37. Aljaafari, A., Sedky, A., Al-Sawalha, A.: *J. Phys. Chem. Solids.* **69**, 2919 (2008)
38. Simon, A., Mukherjee, P.S., Sarma, M.S., Damodaran, A.D.: *J. Mater. Sci.* **29**, 5059 (1994)
39. Halim, S.A., Mohamed, S.B., Azhan, H., Khawaldeh, S.A., Sidek, H.A.A.: *Physica C.* **312**, 78 (1999)
40. Pei, G., Xia, C., Cao, S., Zhang, J., Wu, F., Xu, J.: *JMMM.* **302**(2), 340 (2006)
41. Shan, F.K., Liu, Z.F., Liu, G.X., Lee, W.J., Lee, G.H., Kim, I.S.: *J. Electroceram.* **13**, 195 (2004)
42. El-Desoky, M.M., Ali, M.M., Afifi, G., Imam, H.: *J. Mater. Sci. Mater. Electron.* (11), (2014)
43. Wang, X.S., Wu, Z.C., Webb, J.F., Liu, Z.G.: *Appl. Phys. A Mater. Sci. Process.* **77**, 561–565 (2003)
44. Sedky, A., Abu-Abdeen, M., Almulhem, A.-A.A.: *Physica B.* **388**, 266 (2007)
45. Khalil, S.M., Low, J.: *Temp. Phys.* **143**(112), 31 (2006)
46. Mandel, P., Poddar, A., Ghosh, B., Choudhury, P.: *Phys. Rev. B.* **43**(16), 13102 (1991)
47. Biju, A., Sarun, P.M., Aloysius, R.P.: *Physica C.* **433**, 68 (2007)
48. Chen, W.M., Wu, X.S., Geng, J.F., Chen, J., Chen, D.B., Jin, X., Jiang, S.S.: *J. Supercond.* **10**(1), 41 (1997)
49. Jean, F., Collin, G., Andrieux, M., Blanchard, N., Marucco, J.F.: *Phys. C.* **339**, 269 (2000)
50. Norman, M.R., Ding, H., Randeria, M., Campuzano, J.C., Yokoya, T., Takeuchi, T., Takahashi, T., Mochiku, T., Kadowaki, K., Guptasarma, P., Hinks, D.H.: *Nature.* **392**, 157 (1998)
51. Alldredge, J.W., Lee, J., McElroy, K., Wang, M., Fujita, K., Kohsaka, Y., Taylor, C., Eisaki, H., Uchida, S., Hirschfeld, P.J., Davis, J.C.: *Nat. Phys.* **4**, 319 (2008)
52. Roesera, H.P., Hettfleischa, F., Huberb, F.M., von Schoenermarka, M.F., Steppera, M., Moritza, A., Nikoghosyanc, A.S.: *Acta Astronaut.* **63**, 1372 (2008)
53. Roesera, H.P., Huberb, F.M., von Schoenermarka, M.F., Nikoghosyanc, A.S.: *Acta Astronaut.* **65**, 489–494 (2009)
54. Bernik, S., Hrovat, M., Kolar, D.: *Supercond. Sci. Technol.* **7**, 920 (1994)
55. Honda, T., Wada, T., Sakai, M., Miyanaga, M., Nishikawa, N., Uchida, S., Uchinokawa, K., Tanaka, S.: *Jpn. J. Appl. Phys.* **27**, L545 (1988)
56. Broido, A.: *J Polymar Sci. A-2.* **7**, 1761–1773 (1969)
57. Venkataramani, R., Garg, S.P., Mazumder, S.: *Bull. Mater. Sci.* **14**(3), 665 (1991)
58. Ravi, S., Seshu Bai, V.: *Phys. Rev. B.* **49**, 13082 (1994)
59. Nkum, R.K., Datars, W.R.: *Supercond. Sci. Technol.* **8**, 822 (1995)
60. Sedky, A., Gupta, A., Awana, V.P.S., Narlikar, A.V.: *Phys. Rev. B.* **58**(18), 12495 (1998)
61. A.A. Bahgat, High Tc Updata (USA) Technical Report 6, 19 (1992)
62. Presland, M.R., Tallon, J.L., Buckley, R.G., Liu, R.S., Floer, N.E.: *Physica C.* **176**, 95 (1991)
63. Konsin, P., Sorkin, B.: *Supercond. Sci. Technol.* **13**, 301 (2000)
64. Leenders, A., Ullrich, M., Freyhardt, H.C.: *Physica C.* **279**, 173 (1997)
65. Veerender, C., Dumke, V.R., Nagabhooshanam, M.: *Phys. Status Solid A.* **144**, 199 (1994)
66. Tabor, D.: *The Hardness of Metals.* Clarendon, Oxford (1951)
67. Lawn, B.R., Wilshaw, T.R.: *J. Mater. Sci.* **10**, 1049 (1975)
68. Quinn, J.B., Quinn, G.D.: *J. Mater. Sci.* **32**, 4331 (1997)
69. Dutta, A.K., Narasaiah, N., Chattopadhyaya, A.B., Ray, K.K.: *Ceram. Int.* **27**, 407 (2001)
70. Farber, B.Y., et al.: *Superconductivity.* **4**, 2296 (1991)
71. Fröhlich, F., Grau, P., Grellmann, W.: *Phys. Status Solidi.* **42**, 79 (1997)
72. Li, H., Bradt, R.C.: *J. Mater. Sci.* **22**, 917 (1993)
73. Hays, C., Kendall, E.G.: *Metallography.* **6**(4), 275 (1973)
74. Aydin, H., Cakiroglu, O., Nursoy, M., Terzioglu, C.: *Chin. J. Phys.* **47**(2), 192 (2009)
75. Li, Z., Ghosh, A., Kobayashi, A.S.: *J. Am. Soc.* **72**, 904 (1989)
76. Prabitha, V.G., Biju, A., Abhilash Kumar, R.G., Sarun, P.M., Aloysius, R.P., Syamaprasad, U.: *Physica C.* **433**, 28 (2005)
77. Biju, A., Aloysius, R.P., Syamaprasad, U.: *Physica C.* **440**, 52 (2006)
78. Munakata, F., Kawano, T., Yamauchi, H., Inoue, Y.: *Physica C.* **190**, 471 (1992)

Publisher's note Springer Nature remains neutral with regard to jurisdictional claims in published maps and institutional affiliations.